ROTARY-BALANCE AND STATIC WIND TUNNEL TESTS OF FOREBODY VORTEX CONTROL TECHNIQUES ON AN F/A-18

Brian R. Kramer*, Gerald N. Malcolm†, Carlos J. Suárez‡
Eidetics International, Inc., Torrance, California 90505

and

Kevin D. James§
Sterling Federal Systems, Inc., Palo Alto, California 94303

ABSTRACT

A wind tunnel test program was conducted on a 6% scale F/A-18, to determine the effectiveness of several methods of forebody vortex control for providing increased yaw control at high angles of attack in static conditions and in a rotating flow field. The forebody vortex control configurations that are shown were the best performers from the static test and are comprised of jets, slots, a single rotating nose-tip strake, and the Rhino Horn. All of the devices were found to be effective at producing controlled yawing moments in both directions from the baseline. The slots tended to be more effective on the leeward side during rotation. The single rotating nose-tip strake and the vertical nose strake provided more damping (anti-spin), in their undeflected positions, than the baseline aircraft. Overall, the Rhino Horn had the largest "envelope" of control power available to initiate a velocity-vector roll, or arrest a spin.

NOMENCLATURE

α, AOA	angle of attack, degrees
b	wing span, 2.245 ft
C_l	rolling moment coefficient (body axis)
C_n	yawing moment coefficient (body axis)
C_Y	side force coefficient (body axis)
C_μ	blowing coefficient, $\frac{\dot{m}_j V_j}{qS}$
c, MAC	mean aerodynamic chord, 0.691 ft
δ	vertical nose strake deflection (+, trailing edge left)
δr	rudder deflection (+, trailing edge left)
F.S.	fuselage station, inches on full-scale aircraft
M	Mach number
m_j	mass flow rate, lbm / sec
Φ	azimuth angle (from the windward meridian), degrees
q, Q	free-stream dynamic pressure, lbf / ft^2
ω,w	rotation rate, rad/sec
Rn	Reynolds number
S	reference wing area , 1.44 ft^2
V	free-stream velocity, ft / sec
V_j	blowing jet exit velocity, ft / sec

* Senior Engineer. Senior Member AIAA.
† Vice President, Aeronautics Division. Associate Fellow AIAA.
‡ Senior Engineer. Member AIAA.
§ Aerospace Engineer. Member AIAA.

INTRODUCTION

High angle of attack aerodynamic controls must be effective during dynamic maneuvers as well as in static conditions. Forebody vortex control is primarily useful in providing directional control and initiating and arresting velocity vector rolls. This paper presents the effectiveness of several forebody control schemes in both static conditions and during velocity vector rolls (rotary-balance) in order to assess their effectiveness.

During the static test program, a large matrix of forebody vortex control (FVC) techniques was tested to determine the most effective candidates to use on the rotary balance apparatus[1-3]. The best performing pneumatic and mechanical devices were then tested on the rotary balance.

Rotary-balance experiments determine the forces and moments of a model in a steady rotational motion about the velocity vector at fixed angles of attack and sideslip. The significance of this motion in the early days of rotary-balance testing was to simulate the flow conditions associated with aircraft in a spin motion and determine whether the moments were pro-spin or anti-spin in nature. This was an important test to establish the spin characteristics of an aircraft and to investigate configuration changes to solve any yaw / roll damping problems. This same motion, rotation around the velocity vector, is now considered to be a key maneuver for enhanced agility in combat for modern fighter aircraft. In order to properly assess the control power to produce a robust velocity vector roll (known as a loaded roll because the aircraft is rolling with significant lift forces due to angle of attack), it is necessary to not only determine the yaw and roll moments statically, but dynamically at the appropriate roll rates.

The rotation rate required in the wind tunnel is determined by matching the non-dimensional roll rate, sometimes referred to as the "reduced rotation rate" that is determined by the desired motion of a full-scale aircraft at typical flight conditions. The non-dimensional roll rate is expressed as $\omega b/2V$, where ω is the rotation rate (rad/sec), b is the wing span and V is the free stream velocity. A typical condition for a full-scale F/A-18 of a velocity-vector roll rate of 60°/sec (with up to 60° AOA) and free stream velocity of 150 ft/sec, then the non-dimensional rotation rate around the velocity vector would be 0.1309. For higher velocities, the non-dimensional parameter would be less.

Because of the large volume of data collected, only the lateral / directional coefficients will be shown in this paper. Likewise, only rotary-balance data for 51° AOA will be shown. If more detail is desired, a complete set of data may be found in Ref. 1.

EXPERIMENTAL SETUP

The experiments were conducted in the NASA Ames Research Center 7 x 10 Foot Wind Tunnel. It is a closed-throat, single return atmospheric tunnel. The primary measurements discussed were taken with a 1.5 inch Task Mark IIE six component internal strain gage balance. During the static test, the model was sting mounted at a roll angle of -90° (wings vertical), as shown in Fig. 1, because the wind tunnel's pitch mechanism was a floor mounted turntable. The test was run at a dynamic pressure of 27 psf (approximately 150 ft/sec), and a Reynolds number of 0.92 million per ft (0.636×10^6 based on wing mean aerodynamic chord). The angle of attack was varied from 0° to 60°, and the sideslip angle from 0° to -10°.

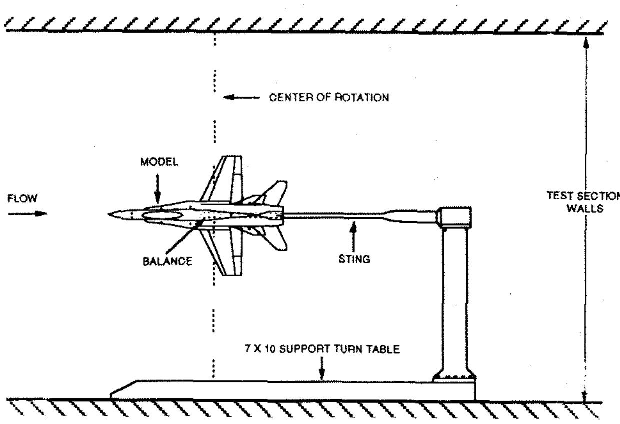

Figure 1: Static Test Installation

The second tunnel entry was a rotary-balance experiment. The rotary rig was based on a unit that was last used in the Ames 6 x 6-Ft Wind Tunnel in 1984. New hardware was designed to provide manual changes in angle of attack by moving and pinning the sting assembly to pre-drilled hole locations (every 3° from 0° to 60°) on the C-strut. The rig was statically balanced with a different counter weight for each angle of attack. Angles of sideslip at specific angles of attack were provided by rolling the straight sting around its own axis in the strut arm in combination with the appropriate angle setting on the C-strut. A rotating seal was designed to allow compressed air to be passed across the rotating junction. The compressed air provided mass flow to the pneumatic forebody controls. The rotary apparatus was mounted in the end of a circular pipe supported by a large A-frame stand (Fig. 2). The hydraulic pump system was located under the test section. The hydraulic and electrical lines were routed to the rig along the top of the cylinder. The balance and instrumentation wires were routed to the model through the center of the cylinder.

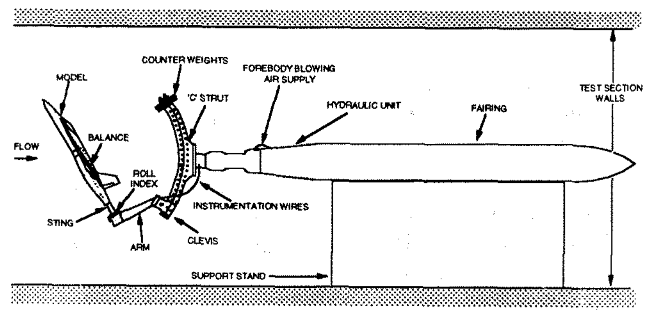

Figure 2: Rotary-Balance Test Installation

The test was run at rotation speeds of -200 (counterclockwise) to 200 (clockwise) rpm ($\omega b/2V = 0.14$), although the rig was later cleared to run up to 350 rpm during an AGARD generic fighter test[4]. As during the static test, most test points were acquired at a dynamic pressure of 27 psf (approximately 150 ft/sec), and a Reynolds number of 0.92 million per ft. (0.636 million based on MAC). Angles of attack of 30°, 45°, 51° and 60° were tested with sideslip angles of 0° and -10° (nose right). Only the data for 51° AOA and 0° sideslip will be presented here.

The test article was a six percent scale model of the F/A-18 (Fig. 3). The model was made by taking a mold of the Navy / MacAir high-speed force and moment wind tunnel model. This mold was used to create a fiberglass shell with the external contours of the aircraft. The underlying structure of the model was a mixture of steel and aluminum in order to carry the loads for both the static and rotary-balance tests. Although the control surfaces were moveable and were tested in their deflected conditions, only the rudder data will be presented here. Because of the very low Reynolds number

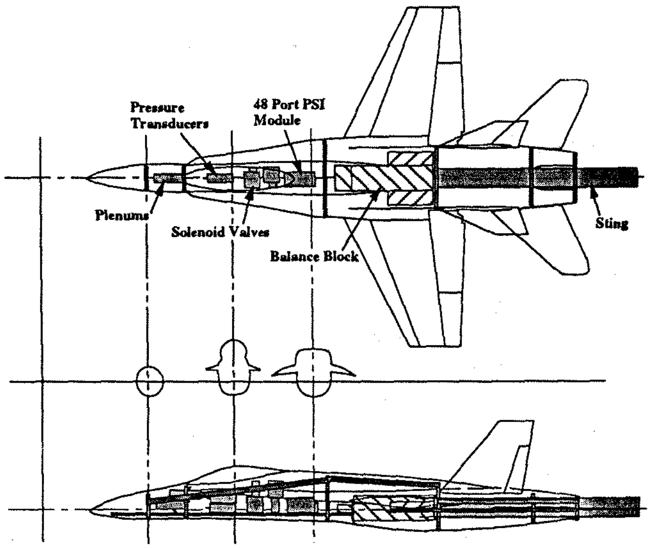

Figure 3: 6% F/A-18 Wind Tunnel Model Details

that the tests were conducted at, the forebody flow was laminar. Experience has shown[5-6] that gritting under these circumstances can cause the flow to experience laminar separation and not model the full scale flow correctly. For this reason, no grit was used for these tests.

The nose section of the model was removable so that different forebody vortex control devices could be studied by replacing the nose section. Although many different devices were tested, only the best performers from each group will be presented here (Fig. 4). The best blowing jet (Fig. 4a) was located at 0.5 equivalent nose diameters aft of the nose tip (1.30 inches model scale) at an azimuth angle of 150°, with the jets pointed 60° inboard from the straight aft position (known as Nose 4-60° Inbd.). The best blowing slot configuration (Fig. 4b) was comprised of segments A and B. The slot was 0.006 inches wide with a length of 1.29 inches beginning 0.66 inches from the nose tip. Only the results from the single rotating nose boom strake (Fig. 4c) will be shown, although two different spacings of dual strakes were also tested and showed good results. Finally, a vertical, pivoting nose strake (the Rhino Horn) was tested as shown in Fig. 4d.

Processing force and moment data from a rotary-balance is similar to standard methods for acquiring data for static tests[7]. The main exception is the need to account for wind-off inertial loads generated by the model during rotation[8].

RESULTS AND DISCUSSION

Baseline Rudder Power

Figure 5 shows the effect of angle of attack on the control power available from the rudder ($\delta r = \pm 30°$). The decrease in yaw control power above 20° AOA is very

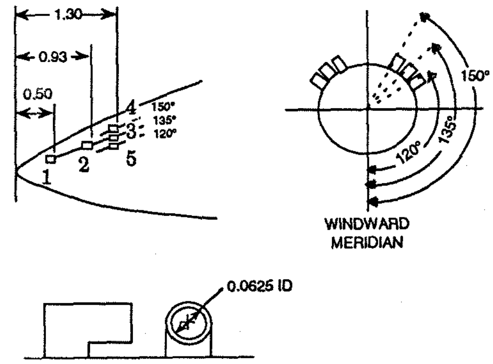

Figure 4a: Jet Blowing Configurations

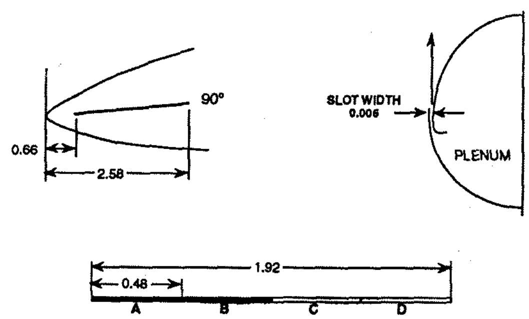

Figure 4b: Slot Blowing Configurations

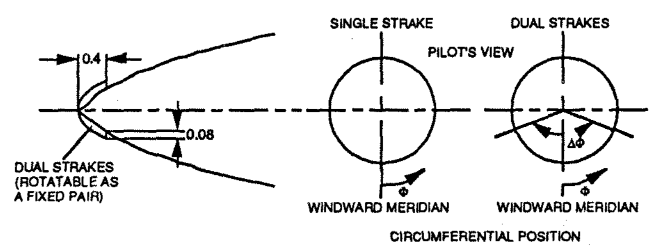

Figure 4c: Rotating Nose Tip Strakes

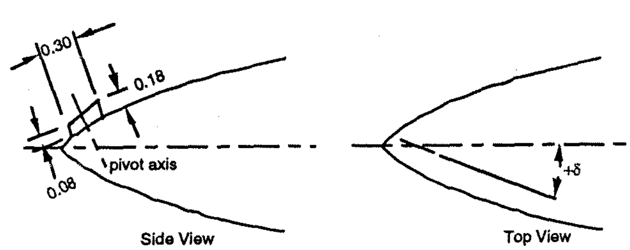

Figure 4d: Rhino Horn

Figure 4: Forebody Vortex Control Devices Tested

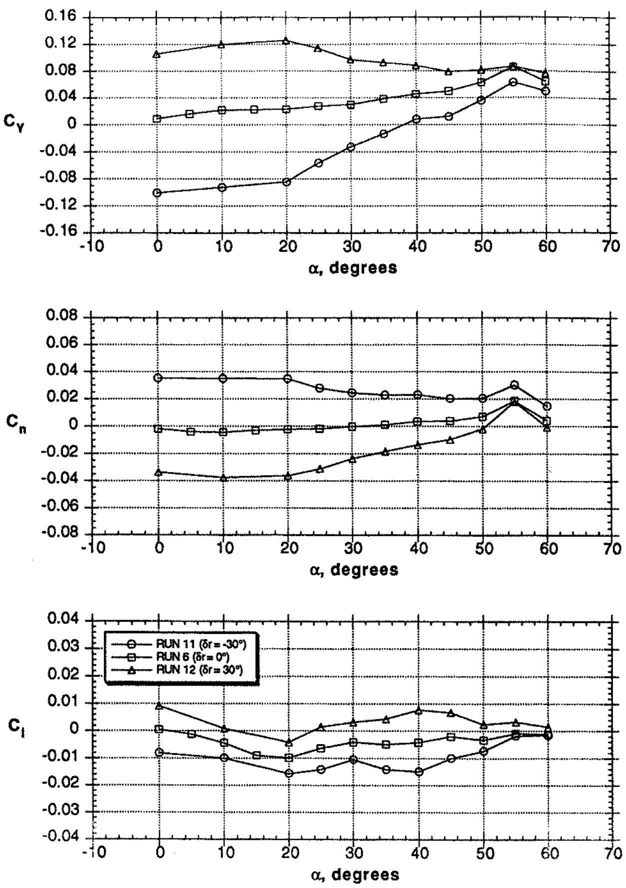

Figure 5: Static Rudder Effectiveness

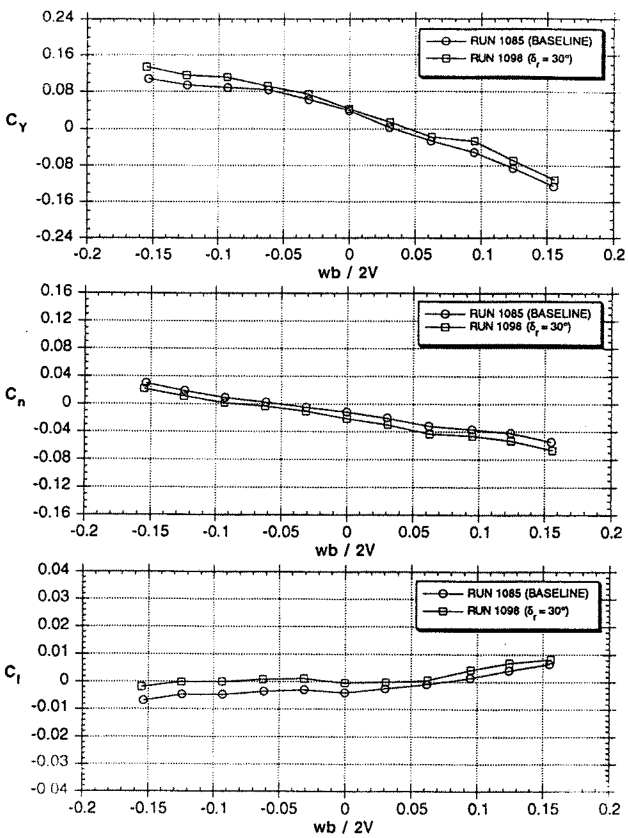

Figure 6: Rudder Effectiveness, α=51°

typical as the vertical tail surfaces are immersed in the wake from the wing. The effect of a rotating flow field on the rudder power ($\delta_r = +30°$) is shown in Fig. 6. The data is for 51° AOA where the rudder is not very effective, however, the rotation rate has very little effect on the level of yaw control. This can be seen as a pure offset from the baseline, without a change in slope.

<u>Jet Blowing at 60° Inboard</u>

Angling the jet blowing nozzles inboard has been shown to greatly increase their effectiveness[9]. During the static test (Fig. 7), Nose 4 with the jets angled inboard 60° provided the best behaved trends with increasing blowing rate beginning at AOA's below 30°. Yawing moment coefficients of ±0.05 were obtained at 50° AOA. This moment is 40% larger than that provided by maximum rudder deflection at 0° angle of attack. With this jet configuration, blowing harder than $C\mu$ = 0.0015 can provide increased yaw power only at angles of attack above 55° and can cause over-blowing at angles below 50°.

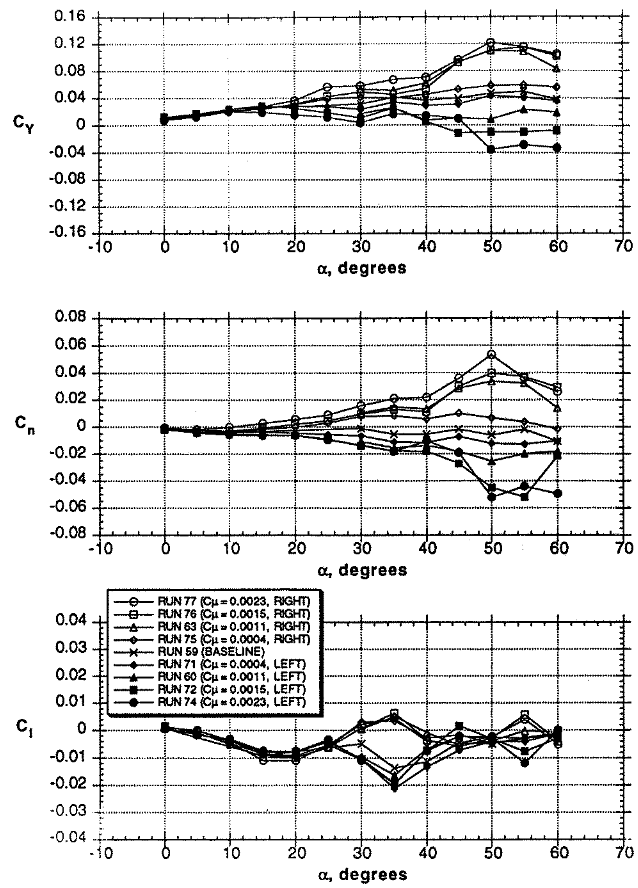

Figure 7: Jet Blowing, Nose 4-60° Inbd.

The effects of rotation rate on jet blowing at an angle of attack of 51° is shown in Fig. 8. Very much like the rudder, the control power available from jet blowing seems to be unaffected by the presence of a rotary flow field (little slope change). There is very little effect on the rolling moment, demonstrating the decoupling of

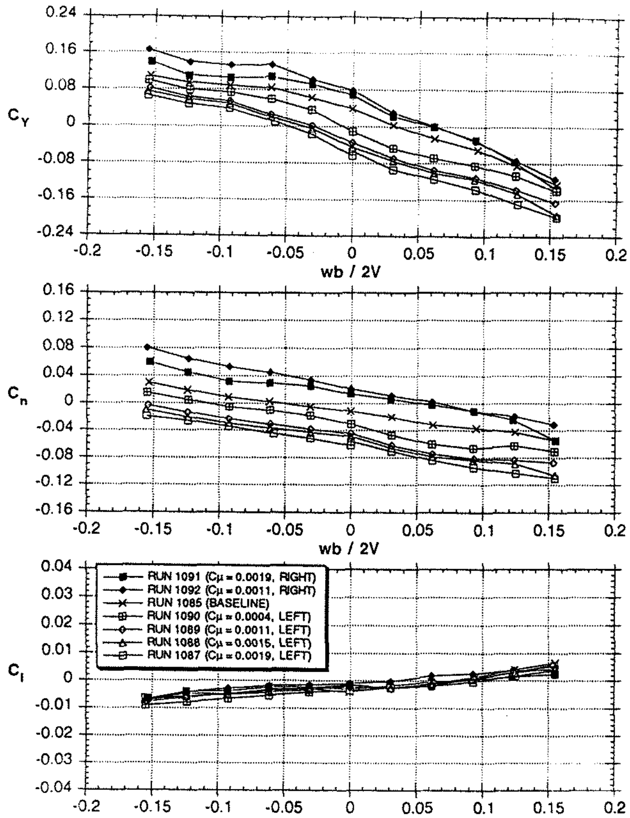

Figure 8: Jet Blowing, Nose 4-60° Inbd., α=51°

the forebody flow field and the LEX flow field at higher angles of attack. The LEX vortices are bursting at the LEX apex at this angle of attack and there is little contribution of the LEX to lift or rolling moment, even if the forebody vortices are asymmetric.

<u>Pressure Distributions</u>

The pressure distribution agreement between the rotary and static tests was excellent, so only the data collected during the rotary test is shown. Figure 9 is a non-rotating case where the effect of the blowing is to increase the level of the suction on the blowing side compared to that on the opposite side. Reversing the side for blowing at the same mass flow rate provides an approximate mirror image response and reverses the pressure distribution. The non-symmetric suction for either left or right blowing, when integrated around the forebody, produces a localized side force, and due to its distance from the CG, a rather large yawing moment. The effect of blowing left and right on the LEX station (F.S. 253) is symmetric about the baseline no-blowing case on the left hand side, but blowing on the left hand side of the forebody produces comparatively larger loss in suction over the right LEX. This increase in suction on the blowing side (left) indicates that the left blowing has moved the right hand vortex away from the surface of the LEX while moving the left hand vortex down closer to the surface. This is exactly the behavior that has

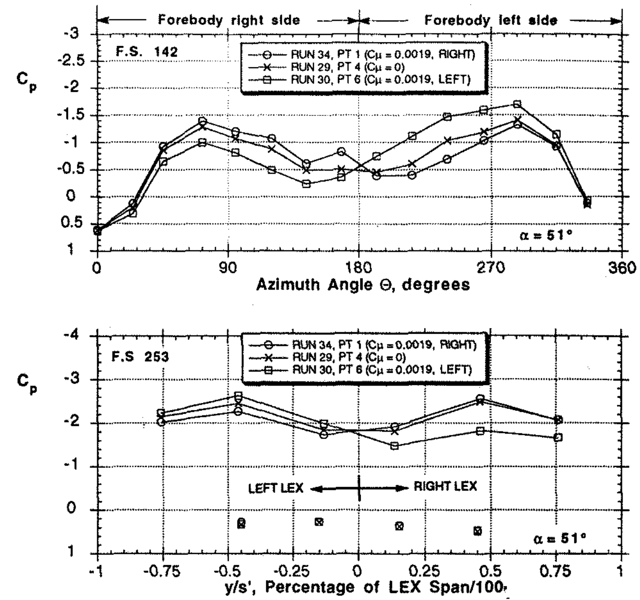

Figure 9: Effect of Cμ, α=50°, ωb/2V=0

been seen in water tunnel dye-flow visualization and wind tunnel smoke tests.

Figures 10 and 11 investigate the effect of jet blowing in rotating flow (w = +0.15 and -0.15 respectively). The baseline shows an increase in the pressure suction peak on the leeward side of the body and a decrease on the windward side. For negative rotation, blowing on the right is nearly identical to the baseline no-blowing case, but blowing on the left shows distinct differences, which agrees with the force data shown in Fig. 8. For positive rotation, blowing left and right produce near mirror image reversals in the pressure distribution. The reason for the difference in the behavior of the pressure distributions for positive and negative rates is not known.

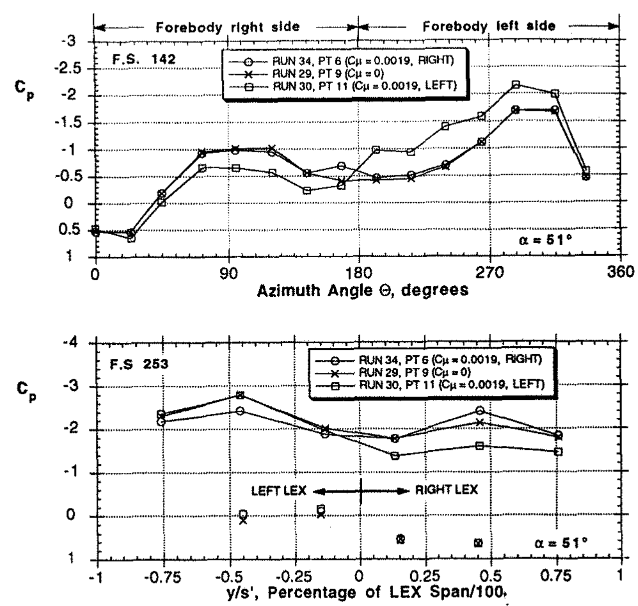

Figure 10: Effect of Cμ, α=50°, ωb/2V=0.15

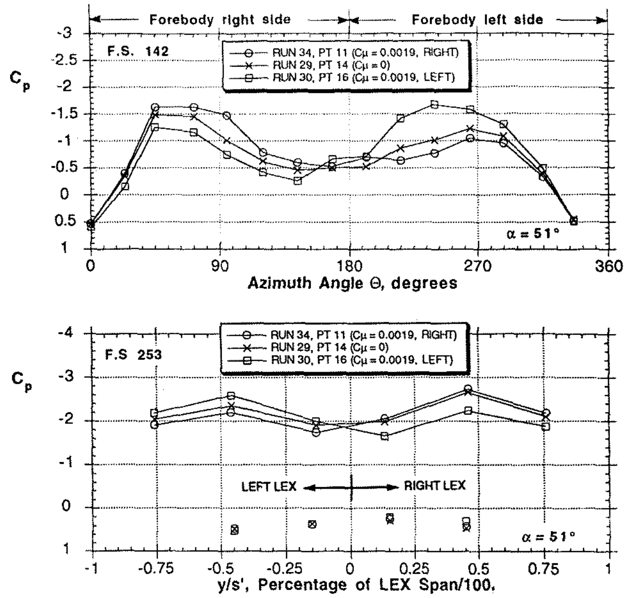

Figure 11: Effect of Cμ, α=50°, ωb/2V=-0.15

Blowing is able to produce changes in the pressure distribution on the forebody and the LEX regardless of the rotation, which agrees well with the force and moment data.

<u>Time Lag Effects - Jet Blowing</u>

An investigation was made to determine whether there is a significant time delay from activation of jet blowing to the time when the aircraft experiences a "fully transitioned" change in the yawing moment. The time lag is important not only for the onset of blowing control, but also for the decay time after the jet is turned off. The time lag was measured by looking at the pressure field response on the surface of the model with Endevco dynamic pressure sensors. In addition, the Task balance outputs were recorded in raw counts, but not reduced to forces or coefficients. As a reference point, the time that it takes the flow to traverse the length of the fuselage (the "convective time") is 22 msec.

Figure 12 shows the jet blowing onset at 50° AOA and a dynamic pressure of 27 psf. When the solenoid valve opens (at 0.065 sec), there is a finite period of time required to establish the plenum pressure (~45 msec). At about 0.090 sec, Endevco #1 begins to respond. Because of the proximity of Endevco #1 on the forebody to the blowing jet, it is apparent that there is a pneumatic lag from not only the plenum filling but also the tubing length from the plenum to the jet exit. By 0.140 sec, Endevco #1 indicates that the flow is fully established at this point on the body. The other Endevcos shown, as well as those not shown, do not sense any change in the flow field caused by the blowing. This is in agreement with the static pressure data discussed above which also saw most of the effect only on the forebody. Perhaps more conclusive evidence of the time lag period is seen by examining the balance output. Here it is clear that by 0.130 sec the new steady state yawing moment has been established. Therefore, a conservative estimate of the time lag for the onset of control (including large pneumatic lags) would be 65 msec (3 convective time units). If the pneumatic lags were removed, the time lag would be on the order of 40 msec or about 2 convective time units. This would be more representative of a full scale aircraft where the control valve could be located near the nozzle exit.

Figure 13 shows time lag associated with the decay of jet blowing at 50° AOA and a dynamic pressure of 27 psf. It took 30 msec for the plenum pressure to bleed down to the static pressure. Even if this lag is included in the total time, the overall lag is only about 80 msec

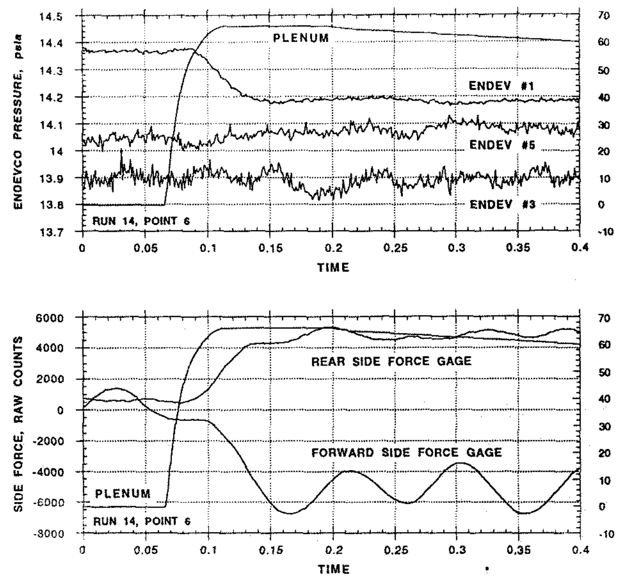

Figure 12: Time Lag-Onset, Jet Blowing, α=50°

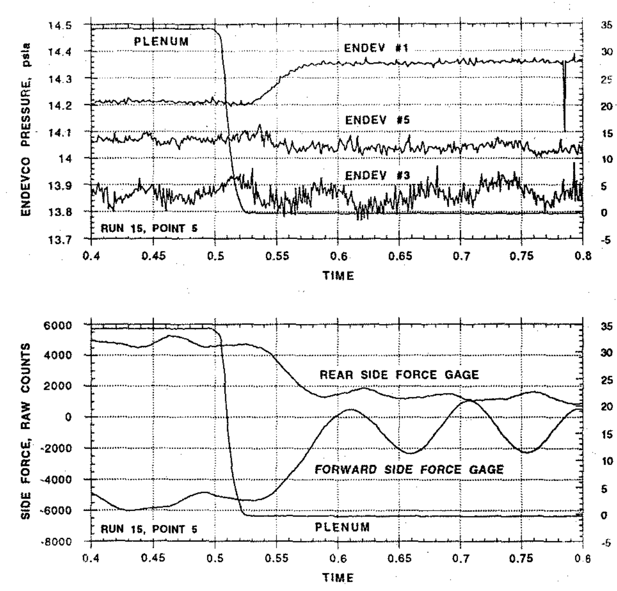

Figure 13: Time Lag-Decay, Jet Blowing, α=50°

(from 0.500 to 0.580). If the pneumatic lag were eliminated, the control lag would be on the order of 60 msec (3 convective time units).

To put these numbers in perspective, the full-scale F/A-18 rudder moves at approximately 70° per second. If the aircraft were flying at 250 ft/sec, one convective time unit would be 0.224 seconds. A full deflection of 30° would take 0.429 seconds, or 2 convective time units.

Slot Blowing

Figure 14 shows yawing moments for segment AB, blowing on the right side only, plotted for various blowing coefficients from 0.0006 to 0.0034. Above 35°, the slot produces more yaw control power than the rudder and reaches an increment of 0.05 (which is 40% greater than the rudder at zero degrees AOA). At low blowing rates (0.0006 and 0.0016) the slot produces yawing moments in the direction away from the side of the forebody that is blowing (right blowing creates negative yaw), but as the blowing rate is increased, the forebody boundary layer flow changes from being disturbed to being entrained and the sign changes so that right blowing gives a positive yawing moment as expected.

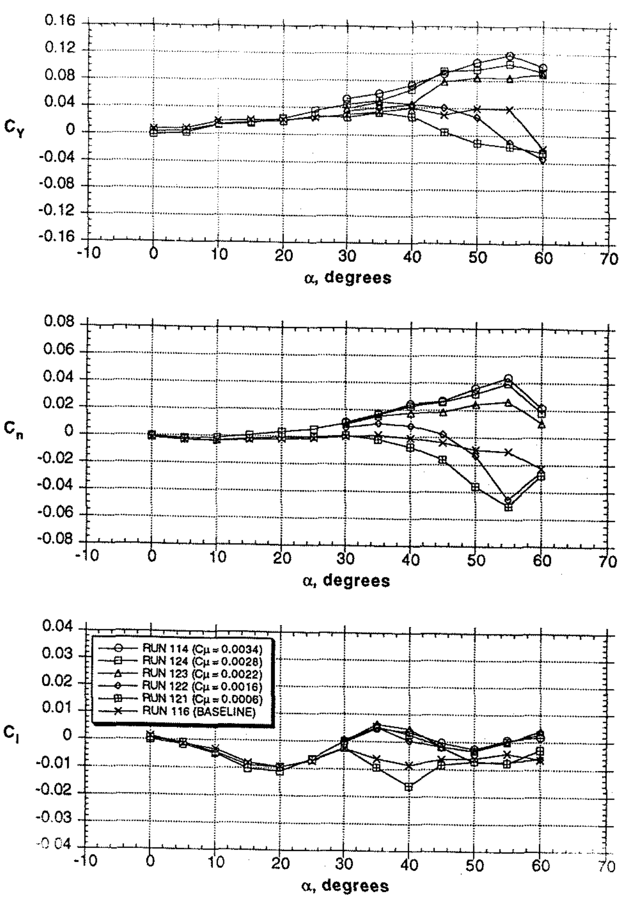

Figure 14: Slot AB Blowing, Right Side Only

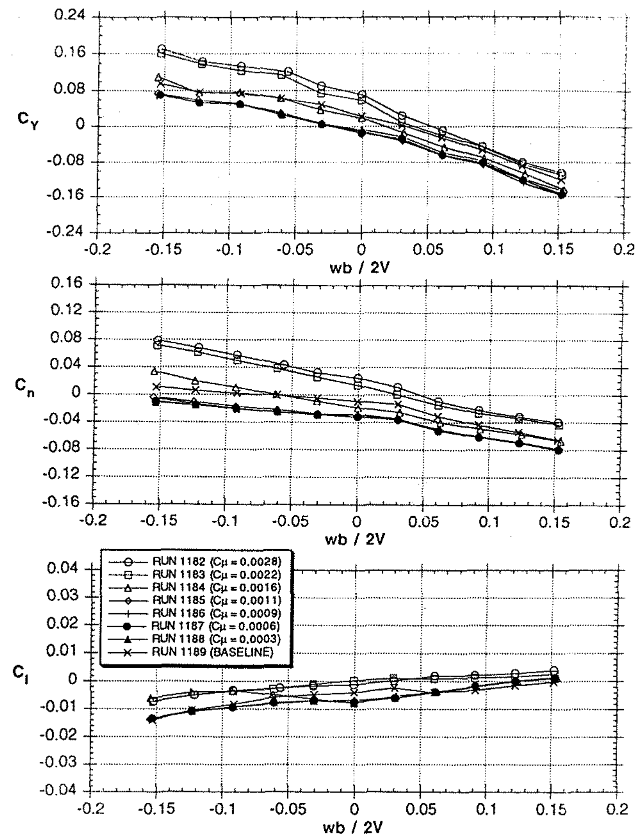

Figure 15: Slot AB Blowing, α=51°

The effect of rotation on the blowing slot, for an angle of attack of 51°, is shown in Fig. 15. As was found in the static tests, the lowest blowing rates at zero rotation rate produce a yawing moment in the opposite direction to the side of the forebody with the slot, and at higher blowing rates the yawing moment change is in the same direction. Also, with blowing on the left (not shown) the effectiveness increases with positive rotation rate and decreases at the highest negative rotation rates, and blowing on the right (Fig. 15) produces the opposite effect, i.e., reduced effectiveness for positive rotation rates and increased effectiveness for negative rotation rates. In other words, the effectiveness is reduced when the side of the forebody with the blowing slot is rotated into the wind and increased when rotated away from the wind. The rolling moment at 51° AOA also shows the reversal in direction with blowing rate but does not seem to change much with rotation rate relative to the baseline configuration.

Single Rotating Nose Tip Strake

With the strake at $\Phi = 180°$ (leeward meridian), the flow field is similar to the baseline flow (Fig. 16). By rotating the strake +/-20° about $\Phi = 180°$ ($160° < \Phi < 200°$), positive and negative yawing moments can be obtained. In general, rotating the strake 20° from the leeward meridian towards the right side of the forebody produces a right-vortex-high pattern, with the corresponding negative or "nose-left" yawing moment. Rotating the strake to the left side of the forebody has the opposite effect and a positive yawing moment is obtained. The changes in yawing moment are well-behaved and are comparable to, and sometimes larger than, the maximum rudder power. At angles of attack lower than 30°, the single strake is not effective. Changes in rolling moment are erratic, but relatively small .

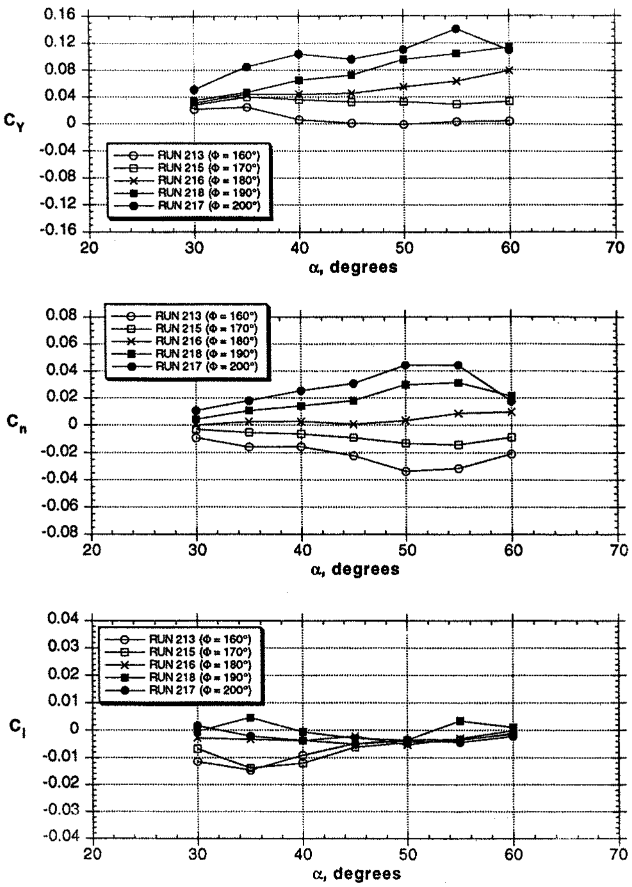

Figure 16: Single Rotating Nose Tip Strake

The performance of a single strake under rotary conditions is shown in Fig. 17. Once again, the angle of attack is 51° and the strake is positioned at various rotation angles from 140° to 220°. The yawing moment coefficient at zero rotation rate shows a negative increment relative to the baseline for Φ = 140° and 160° (clockwise rotation from 180° from pilot's view), and a positive increment for 200° and 220°, as was seen in the static test results. The negative increment for Φ = 140° and 160° increases with negative rotation and decreases with positive rotation, becoming almost zero at the maximum positive rotation rate. The positive increment at zero rotation rate for Φ = 200° and 220° does the opposite. This effect may be a function of the local roll angle of the strake with respect to the wind, which, of course, is changing with rotation rate. It may also be a function of how the forebody vortices react with the rest of the airframe. There is very little effect on the rolling moment.

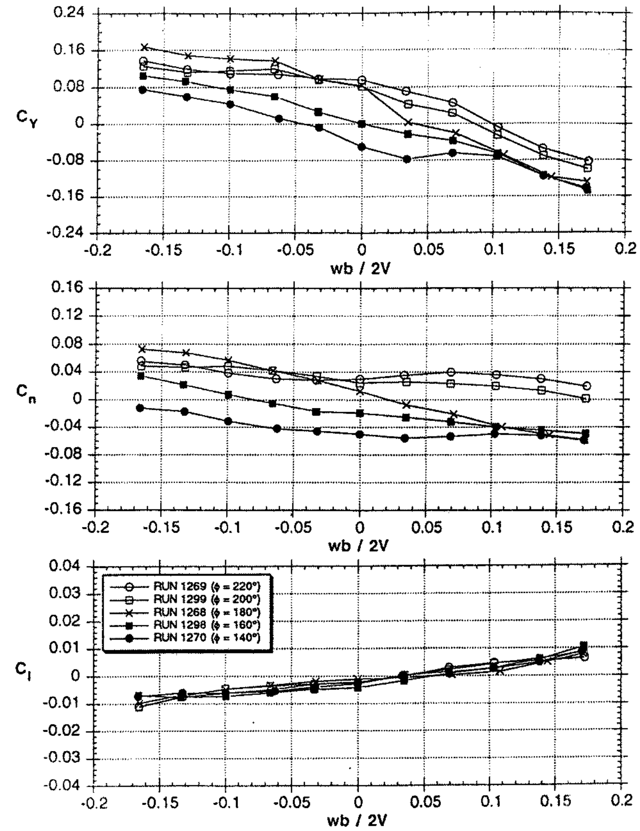

Figure 17: Single Rotating Nose Tip Strake, α=51°

<u>Rhino Horn</u>

The Rhino Horn is a small strake mounted on the leeward side of the forebody near the tip of the nose. The strake pivots about an axis perpendicular to the surface of the forebody. A positive deflection, δ, is defined as trailing edge left, looking from the top. The Rhino Horn proved very effective in manipulating the forebody vortices in preliminary water tunnel tests and, as seen in Fig. 18, it induced large changes in side force and yawing moment during the static test as well. A positive deflection (trailing edge left) produces a positive yawing moment and vice versa. From flow visualization obtained in the water tunnel, when the Rhino Horn is pivoted trailing edge left, a strong vortex forms at the leading edge of the device. This leading edge vortex moves towards the left side of the forebody, and apparently, is increasing the suction on the right side and, at the same time, is pushing the left forebody vortex away from the body surface. This creates a left-vortex-high pattern with the associated positive yawing moment. When the Rhino Horn is pivoted trailing edge right, a negative yawing moment is induced, as seen for the δ = -20°, -36° and -50° cases. As for the rotatable strake case, the changes in rolling moment are small, erratic and depend strongly on angle of attack.

The effect of rotation rate on the aerodynamics of the Rhino Horn, at 51° AOA, is shown in Fig. 19 for several

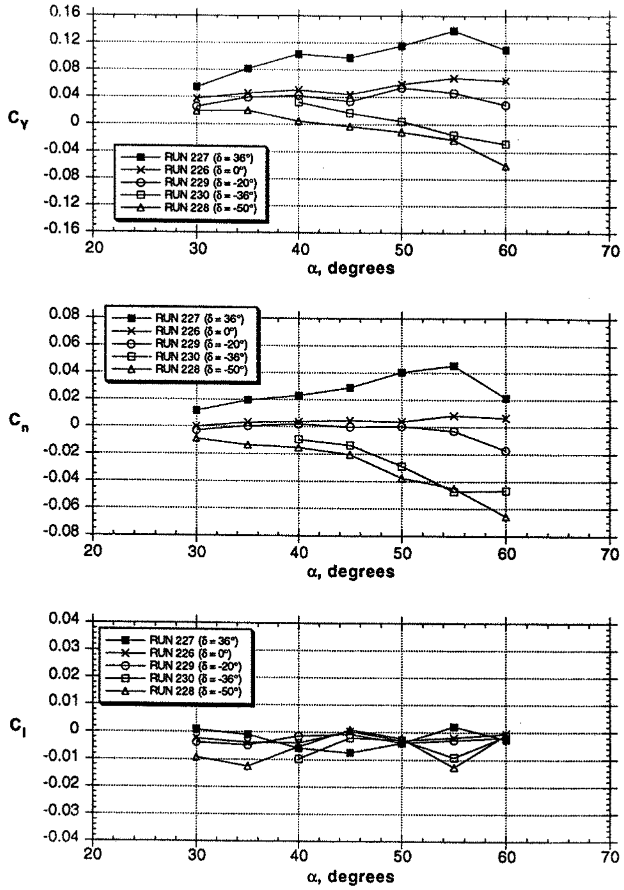

Figure 18: Rhino Horn Effectiveness

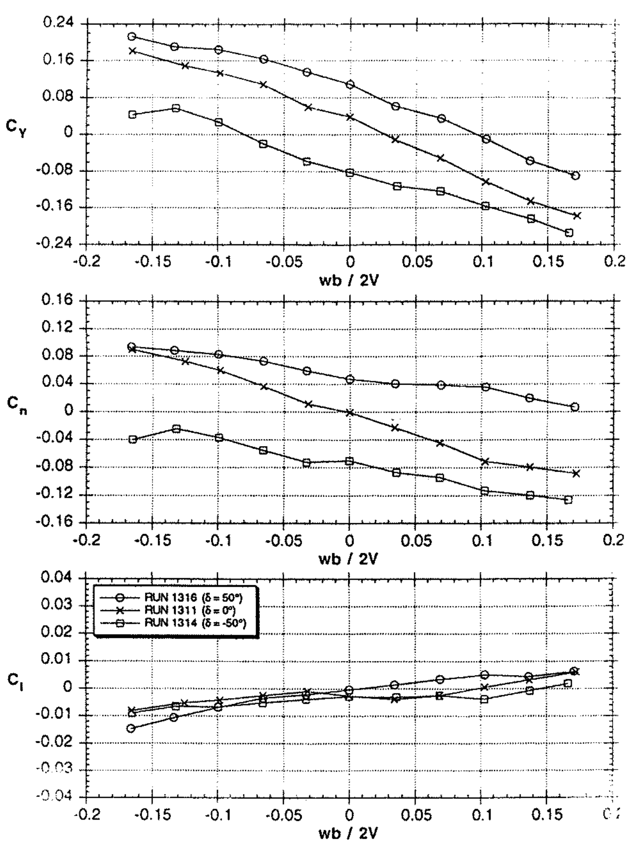

Figure 19: Rhino Horn, α=51°

different deflection angles (trailing edge left is positive). The yawing moment variation at zero rotation rate shows, as was observed in the static tests, that trailing-edge left deflections of +20° and +36° result in positive yawing moments relative to the baseline. Negative deflections result in negative yawing moments. The characteristics of the yawing moment (and side force) with rotation rate are very similar to those observed earlier for the single strake, except that the Rhino Horn produces larger effects. For example, positive deflection provides a positive yawing moment, but the increment decreases with negative rotation rate and increases with positive rates. Negative deflections experience decreasing effectiveness with positive rotation rate and increasing effectiveness with negative rotation rates. The rolling moment shows small effects of strake deflection with rotation rate.

<u>Application to a Future Flight Control System</u>

All of the devices studied (jets, slots, single rotating nose tip strake, and the Rhino Horn) have shown the ability to create large yawing moments in a rotary flow field. The overall effectiveness of each of these devices can be thought of as an envelope of yaw control power (Cn) as a function of non-dimensional spin rate as shown in Fig. 20. The baseline F/A-18 is shown as a single line that indicates that the aircraft would have anti-spin behavior (negative slope). As expected, when jets or slots (non-blowing condition) are added to the aircraft nose, there is little change in the slope of this line (Fig.'s 8 and 15). Blowing at different rates produce the envelope shown in Fig. 20. The single rotating tip strake and the Rhino Horn both cause the aircraft to be even more anti-spin in their undeflected positions (Fig.'s 17 and 19). Their deflected control envelopes are also shown in Fig. 20. Overall, the Rhino Horn produces the largest envelope of effectiveness, as shown by the size of it's shaded area on the diagram.

If a stability augmentation system (SAS) is used in a flight control system, it is clear that the aircraft's anti-spin characteristics can be modified by any of these devices. The envelopes shown in Fig. 20 illustrate the design space that can be generated for each of the

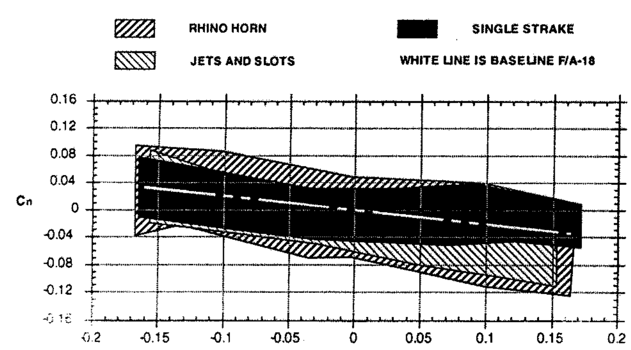

Figure 20: Relative Effectiveness of FVC Methods, α=51°

devices. The flight control engineer can use rate feedback and choose to make the aircraft perform exactly like a standard F/A-18 or design the system to provide more, or less, anti-spin behavior (even to the point of making it pro-spin if desired).

In addition to a SAS, a command augmentation system (CAS) can be designed into the flight control system. This system would blend the forebody vortex control with the conventional aerodynamic surface controls at angles of attack above approximately 30°. The CAS would provide the increased maneuverability that is needed in future fighter aircraft for increased agility at high angles of attack.

CONCLUSIONS

1) Typically, forebody vortex control techniques are effective above 30° AOA.

2) Jet blowing (Nose 4 with nozzles canted 60° inboard) provided the same level of side force and yawing moment observed in the static test, with little degradation at non-dimensional rotation rates as high as 0.28. The level of rolling moment produced is small enough to not be a factor.

3) The time lag between the beginning (onset) of jet blowing and the response of the aircraft is about two convective time units. The lag associated with the shut down (decay) of blowing is about three convective time units. This compares well to the rudder, which takes 2 convective time units to move to full deflection.

4) Slot blowing is more effective on the leeward side of the fuselage during rotation. Blowing on the windward side becomes less effective with higher rotation rates.

5) The single strake, from a baseline of $\Phi = 180°$, produces a negative increment relative to the baseline for $\Phi = 140°$ and 160° (clockwise rotation from 180° from pilot's view) and a positive yawing moment increment for 200° and 220°. The negative increment for $\Phi = 140°$ and 160° increases with negative rotation and decreases with positive rotation, becoming almost zero at the maximum positive rotation rate. The positive increment at zero rotation rate for $\Phi = 200°$ and 220° does the opposite.

6) The Rhino Horn, from a baseline of $\delta = 0°$, produces a positive yawing moment increment for positive (trailing edge left) δ's and a negative yawing moment increment for negative δ's. The positive increment increases with positive rotation and decreases with negative rotation, becoming almost zero at the maximum negative rotation rate. The negative deflection increment does the opposite (similar to the single strake).

7) The vertical nose strake (rhino horn) produced the largest maximum yawing moment increment ($\Delta Cn = -0.13$ at $\omega b/2V = -0.16$) of any device tested.

8) All of the forebody vortex control methods tested appear to be usable in an advanced flight control system as either a SAS or CAS system, or both.

ACKNOWLEDGMENTS

Support for this work was provided by NASA-Ames Research Center under contract NAS2-13383. The technical monitors were Dr. Lewis Schiff and Dr. James Ross. We would like to acknowledge the efforts of Mr. Bert Ayers, of Eidetics International, for his high quality work in constructing the wind tunnel model and refurbishing the rotary rig. In addition we would like to thank Dynamic Engineering, Inc. for their excellent work in fabricating the new rotary balance hardware.

REFERENCES

1. Kramer, B. R., Suárez, C. J., Malcolm, G. N. and Ayers, B. F.; "F/A-18 Forebody Vortex Control," NASA Contractor Report CR-4582 Volumes 1 & 2, March 1994.

2. Kramer, B. R., Suárez, C. J., Malcolm, G. N. and James, K. D.; "Forebody Vortex Control with Jet and Slot Blowing on an F/A-18," AIAA Paper 93-3449, AIAA 11th Applied Aerodynamics Conference, Monterey, CA., Aug. 1993.

3. Suárez, C. J., Kramer, B. R., and Malcolm, G. N.; "Forebody Vortex Control on a F/A-18 Using Small, Rotatable 'Tip-Strakes'," AIAA Paper 93-3450, AIAA 11th Applied Aerodynamics Conference, Monterey, CA., Aug. 1993.

4. Malcolm, G. N., Kramer, B. R., Suárez, C. J., Ayers, B. F. James, K. D., O'Leary, C. O., Wier, B., Walker, J. M.; "US/UK Rotary-Balance Test Comparisons with a Generic Fighter Model," AIAA Paper 94-0196, AIAA 32nd Aerospace Sciences Meeting, Reno, NV., Jan. 1994.

5. Hall, R. M., Banks, D. W., "Progress in Developing Gritting Techniques for High Angle of Attack Flows," AIAA Paper 94-0169, AIAA 32nd Aerospace Sciences Meeting, Reno, NV., Jan. 1994.

6. Banks, D. W., Hall, R. M., Erickson, G. E., Fisher, D. F., "Forebody Flow Field Effects on the High Angle-of-Attack Lateral-Directional Aerodynamics of the F/A-18," AIAA Paper 94-0170, AIAA 32nd Aerospace Sciences Meeting, Reno, NV., Jan. 1994.

7. van Aken, Johannes M., "Description of the Standard Wind Tunnel Balance Program", CRINC Report 7440-3, NASA Grant NCC 2-417, April, 1988.

8. Fluid Dynamics Panel, Advisory Group for Aerospace Research and Development (AGARD), "Rotary-Balance Testing for Aircraft Dynamics," AGARD Advisory Report No. 265, Dec. 1990.

9. Guyton, R. W., Maerki, G., "X-29 Forebody Jet Blowing," AIAA Paper 92-0017, presented at the 30th Aerospace Sciences Meeting, Reno, Nevada, January 1992.

10. Hulzberg, R., "Low Speed Rotary Aerodynamics of F-18 Configuration for 0° to 90° Angle of Attack - Test Results and Analysis," NASA CR 3608, August 1984.

11. Malcolm, G. N., "Forebody Vortex Control - A Progress Review," AIAA Paper 93-3540, Invited Paper, AIAA 11th Applied Aerodynamics Conference, Monterey, CA., Aug. 1993.